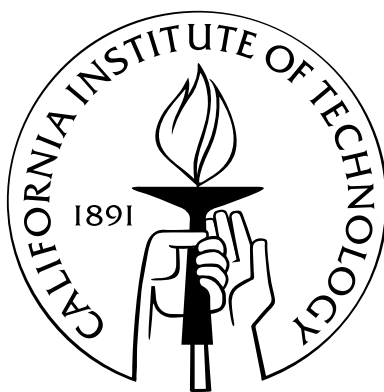


Photochemical and dynamics studies of oxygen isotope exchange reactions of CO₂

Thesis by
Laurence Yip-Lun Yeung

In Partial Fulfillment of the Requirements
for the Degree of
Doctor of Philosophy



California Institute of Technology
Pasadena, California

2010

(Defended December 10, 2009)

© 2010

Laurence Yip-Lun Yeung

All Rights Reserved

Small quantities of different gases were added to separate portions of a non-inflammable mixture of dry carbonic oxide and oxygen, and the spark was then passed. In all cases where a gas containing hydrogen was introduced, the mixture exploded; in all cases where a gas containing no hydrogen was introduced, the mixture did not explode.

— Harold Dixon, *The Combustion of Carbonic Oxide and Hydrogen*, 1886.

Acknowledgements

This body of work would not have been possible without the intellectual, spiritual, and financial support from professor Mitchio Okumura, professor John Eiler, and Dr. William Davidow. Mitchio and John have taught me how to think critically and quantitatively about scientific problems; their unending creativity, enthusiasm, and wisdom continue to inspire me. Dr. Davidow's generous endowment funded all of this research and much more not documented here. Only with his support was I able to pursue these risky projects.

To my collaborators, professors Hagit Affek, Kristie Boering, Elliot Atlas, Tim Minton, Jon Camden, and George Schatz; Drs. Sue Schauffler, Jeff Paci, Weifu Guo, Kate Hoag, and Jianming Zhang; and Mr. Aaron Wiegel: This work was a collective effort, and I dare not take the credit for any more than my own modest contribution to it. Thank you for your time, patience, lab equipment, and fishing lessons.

To the Okumura group, the Eiler group, and other mentors, professors Jack Beauchamp, Rudy Marcus, Geoff Blake, Yuk Yung, Zhengrong Wang, Julie Fry, Rose Came, Kate Huntington, Ben Passey, Naomi Levin, and Aradhna Tripathi; Drs. Pin Chen, Joe Hodges, Chip Miller, Linda Brown, Andrew Mollner, David Robichaud, Aaron Noell, Nathan Eddingsaas, and Mathieu Daëron; Mr. Bill Bing; fellow students Kana Takematsu, Matt Sprague, Kathleen Spencer, Dave Long, Sigrid Barklund, Aileen Hui, Thinh Bui, Nathan Honsowetz, and Heather Widgren: Most of my education here has been at your hands. Thank you for your time, wisdom, skepticism, and coffee.

Finally, to my friends and family: You are the music of my life. You are the rhythm, the harmony, and melody. *If music be the food of love, play on.* Nothing I could say would ever be enough to express my gratitude. I am excited for whatever misadventures lie ahead.

Abstract

This dissertation describes laboratory studies of three oxygen isotope exchange reactions — $O(^1D) + CO_2$, $O_2 + CO_2$, and $O(^3P) + CO_2$ — and their importance to oxygen cycling in the upper atmosphere. First, we studied the isotope exchange reaction $O(^1D) + CO_2$, which is believed to govern the oxygen-isotope budget of CO_2 in the stratosphere. Our combined field, laboratory, and modeling study of the exceptionally rare $^{16}O^{13}C^{18}O$ isotopologue revealed that $O(^1D) + CO_2$ explains only part of the stratospheric CO_2 isotopologue budget, not all of it as previously thought: $O(^1D) + CO_2$ could not explain the large enrichments of $^{16}O^{13}C^{18}O$ (i.e., of the “ Δ_{47} ” tracer) at high Northern latitudes. Mesospheric and heterogeneous chemistry of CO_2 were proposed as possible sources of this meridional variation in $^{16}O^{13}C^{18}O$. Therefore, we performed crossed-molecular-beam experiments to investigate the chemistry of CO_2 at hyperthermal collision energies; this class of reaction could be important in the upper atmosphere, where low gas densities and high rates of photochemistry increase the relative probability of hyperthermal reactions. Our experimental and theoretical study of the $O_2 + CO_2$ isotope exchange reaction showed that the reaction can occur through a short-lived CO_4 reaction complex, which leads to $O_2 + CO_2$ products that are highly internally excited, but possibly still in their ground electronic state. Our study of $O(^3P) + CO_2$ collisions at hyperthermal energies showed that $O(^3P) + CO_2$ isotope exchange can occur in the upper atmosphere, proceeding through a short-lived CO_3 reaction complex. The $O(^3P) + CO_2 \rightarrow O_2 + CO$ reaction was also observed, and our data suggest that it can proceed through a ‘stripping’ mechanism or a CO_3 complex. These reactions demonstrate new ways in which oxygen can be cycled through CO_2 in the atmosphere; their isotope effects, manifest in the isotopic composition of atmospheric CO_2 , may impose independent constraints on atmospheric transport and biosphere-atmosphere interactions.

Contents

| | |
|--|-----------|
| Acknowledgements | iv |
| Abstract | v |
| 1 Introduction | 1 |
| 1.1 CO ₂ in the global carbon cycle | 1 |
| 1.2 Stable isotopes, ‘clumped’ and otherwise | 2 |
| 1.3 Anomalous isotopic enrichments in stratospheric CO ₂ | 2 |
| 1.4 Insights from the physical chemist’s toolbox | 5 |
| 1.5 Executive summary | 8 |
| Appendices | 9 |
| 1.A Isotopic notation | 10 |
| 1.B Copyright declaration | 12 |
| 2 Large and unexpected enrichment in stratospheric ¹⁶O¹³C¹⁸O | 13 |
| 2.1 Abstract | 14 |
| 2.2 Introduction | 15 |
| 2.3 Field sample collection and analysis | 16 |
| 2.4 Field results | 17 |
| 2.5 Laboratory photochemical experiments | 18 |
| 2.5.1 ¹³ C/ ¹² C kinetic isotope effect experiments | 21 |
| 2.5.2 Continuous-irradiation experiments | 32 |
| 2.5.3 Conclusions from laboratory measurements | 34 |
| 2.6 Discussion | 36 |
| 2.6.1 O(¹ D)+CO ₂ only explains mid-latitude ¹⁶ O ¹³ C ¹⁸ O variations | 36 |
| 2.6.2 Effects of intra-stratospheric chemistry and mixing | 37 |
| 2.6.3 Effects of mesospheric and heterogeneous chemistry | 39 |
| 2.7 Conclusions | 47 |
| 2.8 Acknowledgements | 47 |
| Appendices | 49 |
| 2.A Mixing effects on isotopic composition | 50 |
| 2.B Practical considerations | 52 |
| 2.B.1 IRMS long-term signal stability | 52 |
| 2.B.2 IRMS vs. optical methods | 53 |
| 2.C Low-temperature cell for ¹³ C/ ¹² C KIE experiments | 58 |
| 2.D MATLAB code for hard-sphere collision model | 67 |

| | | |
|----------|---|------------|
| 2.D.1 | montecarlo.m | 67 |
| 2.D.2 | scatter.m | 69 |
| 3 | A hyperthermal O-atom exchange reaction, O₂ + CO₂ | 71 |
| 3.1 | Abstract | 72 |
| 3.2 | Introduction | 73 |
| 3.3 | Experimental studies | 73 |
| 3.3.1 | Methods | 73 |
| 3.3.2 | Results | 80 |
| 3.4 | Theoretical studies | 87 |
| 3.5 | Proposed mechanism | 89 |
| 3.6 | Conclusion | 92 |
| 3.7 | Acknowledgements | 93 |
| | Appendices | 95 |
| 3.A | Non-reactive scattering of O ₂ and CO ₂ | 96 |
| 3.B | MATLAB program for generating Newton diagrams | 101 |
| 3.B.1 | NewtonD.m | 101 |
| 3.B.2 | NewtonDcalc.m | 103 |
| 3.B.3 | NewtonDplot.m | 104 |
| 4 | Dynamics of O(³P) + CO₂ collisions at hyperthermal energies | 109 |
| 4.1 | Abstract | 110 |
| 4.2 | Introduction | 111 |
| 4.3 | Theoretical studies | 113 |
| 4.3.1 | Electronic structure calculations | 113 |
| 4.3.2 | Reaction dynamics calculations | 118 |
| 4.4 | Experimental studies | 123 |
| 4.4.1 | Methods | 123 |
| 4.4.2 | Results | 125 |
| 4.5 | Discussion | 139 |
| 4.5.1 | Theoretical studies | 139 |
| 4.5.2 | Non-reactive scattering of O(³ P) and CO ₂ | 141 |
| 4.5.3 | Oxygen isotope exchange, O(³ P) + CO ₂ → O + CO ₂ | 142 |
| 4.5.4 | Oxygen-atom abstraction, O(³ P) + CO ₂ → O ₂ + CO | 144 |
| 4.6 | Conclusions | 147 |
| 4.7 | Acknowledgements | 148 |
| | Appendices | 149 |
| 4.A | Differential scattering cross-sections from 1.0 – 6.5 eV | 150 |
| 4.B | Estimating uncertainty in the laboratory angular distributions | 152 |
| 5 | Summary and outlook | 153 |
| 5.1 | New signatures, new reactions | 153 |
| 5.2 | Potential atmospheric importance of O(³ P) + CO ₂ | 154 |
| | Bibliography | 157 |

List of Figures

| | | |
|------|---|----|
| 1.1 | Schematic of atmospheric CO ₂ sources and sinks. | 3 |
| 1.2 | Bulk oxygen isotope composition of stratospheric CO ₂ | 5 |
| 1.3 | Potential energy surface for CO ₃ (³ A'') from <i>Mebel et al.</i> [2004]. | 6 |
| 2.1 | Meridional variation of Δ ₄₇ measured in stratospheric samples. | 18 |
| 2.2 | Correlation between Δ ₄₇ and stratospheric tracers. | 19 |
| 2.3 | Δ ¹⁷ O values vs. long-lived stratospheric tracer mixing ratios. | 19 |
| 2.4 | Schematic of O(¹ D) + CO ₂ reaction-purification-analysis procedure. | 21 |
| 2.5 | FT-IR spectrum of synthesized N ₂ ¹⁸ O between 1100 cm ⁻¹ and 4000 cm ⁻¹ | 24 |
| 2.6 | Modeled O(¹ D) + CO ₂ reaction collision energy distributions at different He bath gas pressure (T = 300 K). | 29 |
| 2.7 | Changes in Δ ₄₇ vs. Δδ ¹⁸ O after pulsed UV photolysis at 300 K and 229 K. | 30 |
| 2.8 | Changes in Δ ₄₇ vs. Δ ¹⁷ O of CO ₂ after continuous UV irradiation of O ₂ /O ₃ /CO ₂ mixtures with a Hg lamp. | 34 |
| 2.9 | How mixing two arbitrary reservoirs of CO ₂ can be nonlinear in Δ ₄₇ | 51 |
| 2.10 | Allan-variance plot of Δ ₄₇ over 40 IRMS acquisitions. | 53 |
| 2.11 | Schematic of conflat chamber used for low-temperature ¹³ C/ ¹² C KIE experiments. | 59 |
| 2.12 | Photograph of conflat chamber used for low-temperature ¹³ C/ ¹² C KIE experiments. | 59 |
| 2.13 | Cold cell assembly. | 61 |
| 2.14 | Machining diagram for the OFHC copper tube. | 61 |
| 2.15 | Machining diagram for the OFHC copper conduction block. | 62 |
| 2.16 | Machining diagram for the OFHC copper heat transfer block. | 63 |
| 2.17 | Machining diagram for the brass heat transfer block. | 63 |
| 2.18 | Machining diagram for the OFHC copper connection to the liquid N ₂ feedthrough. | 64 |
| 2.19 | Cold cell assembly for O(¹ D), OH + CH ₄ KIE experiments. | 65 |
| 2.20 | Machining diagram illustrating the modifications made to the conduction block for O(¹ D), OH + CH ₄ KIE experiments. | 65 |
| 2.21 | Machining diagram for the OFHC copper heat transfer block designed for O(¹ D), OH + CH ₄ KIE experiments. | 66 |
| 3.1 | Crossed-molecular-beam apparatus with hyperthermal oxygen source. | 74 |
| 3.2 | Canonical Newton diagram for hyperthermal ¹⁶ O ₂ + ¹² C ¹⁸ O ₂ collisions. | 75 |
| 3.3 | Velocity distribution of hyperthermal oxygen beam. | 77 |
| 3.4 | Laboratory TOF distribution of <i>m/z</i> = 46 (¹⁶ O ¹² C ¹⁸ O ⁺) at Θ = 6°, with the inelastic scattering signal removed. | 80 |

| L. Y. Yeung | Oxygen isotope exchange reactions of CO ₂ | Figures |
|-------------|---|---------|
| 3.5 | TOF distributions for ¹⁶ O ¹² C ¹⁸ O products at laboratory angles $\Theta = 6^\circ$ and 8° with the inelastic scattering signal removed. | 82 |
| 3.6 | TOF distributions for ¹⁶ O ¹² C ¹⁸ O ($m/z = 46$) at various laboratory angles Θ with the inelastic scattering signal removed. | 83 |
| 3.7 | Center-of-mass-frame (A) angular and (B) translational energy distributions from the ¹⁶ O ₂ + ¹² C ¹⁸ O ₂ oxygen isotope exchange reaction obtained from TOF fits of $m/z = 46$ | 84 |
| 3.8 | Velocity-flux contour diagram for ¹⁶ O ¹² C ¹⁸ O products of ¹⁶ O ₂ + ¹² C ¹⁸ O ₂ collisions in the center-of-mass frame. | 84 |
| 3.9 | Energetically allowed neutral product channels from O ₂ + CO ₂ collisions. . . | 86 |
| 3.10 | Calculated energies and structures on the lowest triplet PES of O ₂ + CO ₂ . . . | 87 |
| 3.11 | Calculated stationary point geometries on the lowest triplet PES of CO ₄ . . . | 89 |
| 3.12 | Calculated energies and structures on the lowest triplet PES of O ₂ + CO ₂ . . . | 89 |
| 3.13 | Singly-occupied molecular orbitals (SOMOs) in the CO ₄ (³ A'') and TS3 structures. | 90 |
| 3.14 | Molecular orbital diagrams for O ₂ and CO ₂ , adapted from <i>DeKock and Gray</i> [1980]. | 91 |
| 3.15 | Electron-pushing diagram of an adiabatic CO ₄ (³ A'') isomerization through TS3. . . | 92 |
| 3.16 | Laboratory scattering data detected at $m/z = 32$ | 98 |
| 3.17 | Laboratory inelastic scattering data detected at $m/z = 48$ | 99 |
| 3.18 | Velocity-flux contour diagram for inelastically scattered ¹² C ¹⁸ O ₂ from ¹⁶ O ₂ + ¹² C ¹⁸ O ₂ collisions in the center-of-mass frame. | 100 |
| 3.19 | Sample output of the <i>NewtonD.m</i> program. | 101 |
| 4.1 | Stationary-point structures for O(³ P) + CO ₂ reactions below 100 kcal mol ⁻¹ calculated at the CCSD(T)/aug-cc-pVTZ level of theory on the ³ A'' surface. . . | 114 |
| 4.2 | Comparison of CO ₃ stationary point geometries relevant to the QCT calculations. . . | 116 |
| 4.3 | Comparison of TS1 and TS3 geometries and energies at various levels of theory. . . | 116 |
| 4.4 | Reactive scattering cross-sections for the O(³ P) + CO ₂ isotope exchange reaction obtained from the QCT calculations. | 121 |
| 4.5 | Opacity functions for the O(³ P) + CO ₂ isotope exchange reaction and for inelastic scattering of the two reagents obtained from QCT calculations at the B3LYP/6-311G(d) and BMK/6-311G(d) levels of theory. | 122 |
| 4.6 | Canonical Newton diagram for ¹⁶ O + ¹² C ¹⁸ O ₂ collisions at $E_{\text{coll}} = 98.8$ kcal mol ⁻¹ | 124 |
| 4.7 | Laboratory inelastic scattering data detected at $m/z = 16$ | 126 |
| 4.8 | Laboratory inelastic scattering data detected at $m/z = 48$ | 128 |
| 4.9 | Velocity-flux contour diagram for inelastically scattered ¹² C ¹⁸ O ₂ from ¹⁶ O(³ P) + ¹² C ¹⁸ O ₂ collisions in the center-of-mass frame. | 129 |
| 4.10 | Comparison of laboratory and theoretical c.m. (A) angular and (B) translational energy distributions for inelastic scattering of O(³ P) and CO ₂ at $\langle E_{\text{coll}} \rangle \approx 100$ kcal mol ⁻¹ | 130 |
| 4.11 | Laboratory reactive scattering data detected at $m/z = 46$ | 132 |
| 4.12 | Velocity-flux contour diagram for ¹⁶ O ¹² C ¹⁸ O products of ¹⁶ O(³ P) + ¹² C ¹⁸ O ₂ collisions in the center-of-mass frame. | 133 |
| 4.13 | Comparison of laboratory and theoretical c.m. (A) angular and (B) translational energy distributions for the O(³ P) and CO ₂ isotope exchange reaction at $\langle E_{\text{coll}} \rangle \approx 100$ kcal mol ⁻¹ | 134 |

| | | |
|------|---|-----|
| 4.14 | Laboratory reactive scattering data detected at $m/z = 34$ | 136 |
| 4.15 | Snapshots of a quasiclassical trajectory for O(³ P) + CO ₂ isotope exchange through a short-lived CO ₃ * complex at 1.5 eV (34.6 kcal mol ⁻¹) collision energy.142 | |
| 4.16 | Laboratory reactive scattering data detected at $m/z = 46$, fit assuming an ISC mechanism. | 145 |
| 4.17 | Snapshots of quasiclassical trajectories for the O(³ P) + CO ₂ → O ₂ + CO reaction.146 | |
| 4.18 | Center-of-mass angular and translational energy distributions for the O(³ P) + CO ₂ isotope exchange reaction derived from QCT calculations at the (A and B) B3LYP/6-311G(d) and (C and D) BMK/6-311G(d) levels of theory. | 151 |

List of Tables

| | | |
|-----|--|-----|
| 2.1 | Stratospheric air sample data | 17 |
| 2.2 | IR band assignments for the spectra in Figure 2.5 | 23 |
| 2.3 | IRMS ion signals from the synthesized N ₂ ¹⁸ O | 25 |
| 2.4 | Results of pulsed photochemical experiments | 30 |
| 2.5 | Results of continuous irradiation experiments | 33 |
| 2.6 | Tropospheric-stratospheric-mesospheric mixing model results | 41 |
| 3.1 | Energies of stationary points associated with the exchange reaction O ₂ + CO ₂ → O ₂ + CO ₂ on the lowest triplet potential energy surface | 88 |
| 4.1 | Energies (kcal mol ⁻¹) for the stationary points on the lowest triplet CO ₃ po- tential energy surface for ¹⁶ O(³ P) + ¹² C ¹⁶ O ₂ → ¹⁶ O + ¹² C ¹⁶ O ₂ collisions . . . | 115 |
| 4.2 | Number of reactive QCTs observed at different collision energies. | 121 |
| 4.3 | Comparison of experimental and theoretical yields for the products of O(³ P) + CO ₂ collisions near 100 kcal mol ⁻¹ | 137 |